Adsorption (2011) 17: 179–188
DOI 10.1007/s10450-010-9298-y

Capture of CO_2 from flue gas by vacuum pressure swing adsorption using activated carbon beads

Chunzhi Shen · Jianguo Yu · Ping Li · Carlos A. Grande · Alirio E. Rodrigues

Received: 14 May 2010 / Accepted: 19 November 2010 / Published online: 11 December 2010

Abstract Vacuum pressure swing adsorption (VPSA) for CO_2 capture has attracted much research effort with the development of the novel CO_2 adsorbent materials. In this work, a new adsorbent, that is, pitch-based activated carbon bead (AC bead), was used to capture CO_2 by VPSA process from flue gas. Adsorption equilibrium and kinetics data had been reported in a previous work. Fixed-bed breakthrough experiments were carried out in order to evaluate the effect of feed flowrate, composition as well as the operating pressure and temperature in the adsorption process. A four-step Skarstrom-type cycle, including co-current pressurization with feed stream, feed, counter-current blowdown, and counter-current purge with N_2 was employed for CO_2 capture to evaluate the performance of AC beads for CO_2 capture with the feed compositions from 15–50% CO_2 balanced with N_2. Various operating conditions such as total feed flowrate, feed composition, feed pressure, temperature and vacuum pressure were studied experimentally. The simulation of the VPSA unit taking into account mass balance, Ergun relation for pressure drop and energy balance was performed in the gPROMS using a bi-LDF approximation for mass transfer and Virial equation for equilibrium. The simulation and experimental results were in good agreement. Furthermore, two-stage VPSA process was adopted and high CO_2 purity and recovery were obtained for post-combustion CO_2 capture using AC beads.

Keywords Vacuum pressure swing adsorption · Activated carbon beads · CO_2 adsorption · Simulation · Breakthrough curve

C. Shen · J. Yu (✉) · P. Li
State Key Laboratory of Chemical Engineering, College of Chemical Engineering, East China University of Science and Technology, Shanghai 200237, China
e-mail: jgyu@ecust.edu.cn

C. Shen · C.A. Grande · A.E. Rodrigues
Laboratory of Separation and Reaction Engineering (LSRE), Associate Laboratory LSRE/LCM, Department of Chemical Engineering, Faculty of Engineering, University of Porto, Rua Dr. Roberto Frias, s/n, 4200-465, Porto, Portugal

1 Introduction

With the concern of increased global warming, more and more attention has been paid to CO_2 capture from flue gases emitted by power plants which account for a large percentage of CO_2 emission (IPCC report 2005). Among the various capture approaches, monoethanolamine (MEA) chemical absorption, membranes, cryogenic, adsorption and others are being considered, CO_2 capture by vacuum pressure swing adsorption (VPSA) is a promising option for separating CO_2 from flue gas since it has a number of advantages, such as possible low energy requirement, low capital investment cost and easy to achieve automated operation (Aaron and Tsouris 2005; Chaffee et al. 2007; Chue et al. 1995; Diagne et al. 1995; Ho et al. 2008; Kikkinides et al. 1993). Particularly, VPSA process with the use of novel CO_2 adsorbents materials has attracted much research effort (Ciferno et al. 2009; Zhang et al. 2008).

There are many potential candidate adsorbent materials available to post-combustion CO_2 capture. Among all alternatives carbonaceous materials are promising adsorbents, since they have high BET surface area, good CO_2 adsorption capacity, they are water tolerant and they can be produced with novel morphologies (monolith, bead, fiber, granular, respectively). Additionally, they are less expensive than other adsorbents like zeolites (Radosz et al. 2008). Activated carbon (AC) beads are spherical and no binder material was used in their production. The spherical nature and

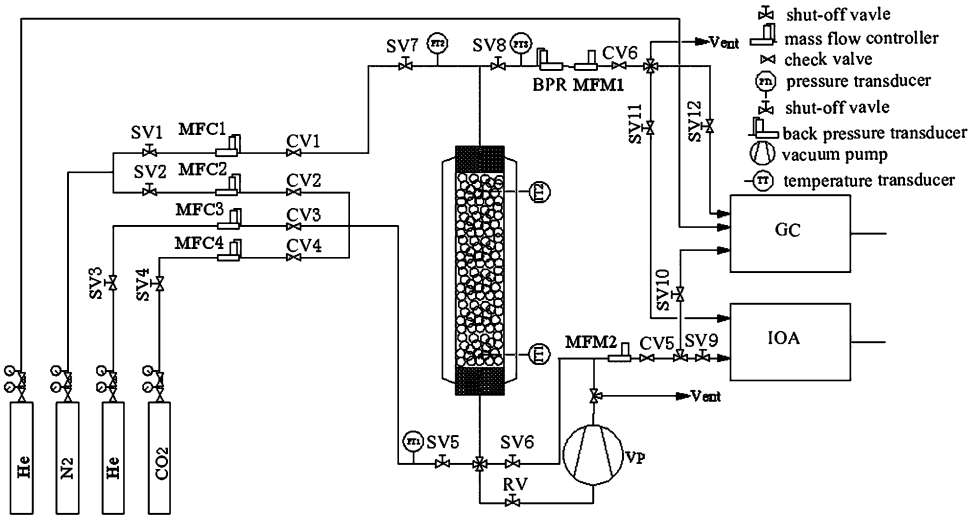

Fig. 1 Scheme of the VPSA apparatus used to study CO_2/N_2 separation with AC beads

hardness of AC bead minimizes dust formation and attrition losses during adsorption and regeneration processes. AC beads also exhibit excellent fluidization properties both in gas and liquid applications. These characteristics make AC bead the material of choice for higher performance in carbonaceous materials application.

The AC beads used in this work were pitch-based synthesized from coal tar pitch through the emulsion method without using binder material by the cooperators in State Key laboratory, China (Liu et al. 1999). In a previous paper, adsorption equilibrium isotherms and adsorption kinetics of CO_2 and N_2 on the AC beads were reported. Preferential adsorption of CO_2 and good kinetics of both CO_2 and N_2 were observed in the AC beads (Shen et al. 2010). The purpose of this paper is to evaluate the performance of a VPSA unit using the new AC beads for CO_2 capture from flue gas. A four-step Skarstrom-type cycle, comprising co-current pressurization with feed stream, feed, counter-current blowdown, and counter-current purge with N_2, was employed for CO_2 capture. Fixed-bed breakthrough experiments were performed at different conditions to review the behavior of the new VPSA unit and to test the validity of the proposed mathematical model under different conditions. The effects of different operation conditions (feed pressure, feed concentration, total feed flowrate, operating temperature and evacuation pressure) in the VPSA process performance were studied experimentally and theoretically.

2 Experimental

2.1 Experimental setup

The experimental VPSA setup is shown in Fig. 1. It contains three main sections:

(1) The mixture section consists of a pressure transducer, four shut-off valves, four check valves, and four mass-flow controllers, MFC1, MFC2, MFC3 and MFC4, connected to nitrogen (MFC1 for purge and MFC2 for feed), helium and carbon dioxide cylinders. The pressure transducer PT1 is from AUTEC (China), with linear pressure response from 0 to 500 kPa, which is located to measure the mixture feed pressure. The four shut-off valves and five check valves are all from Swagelok. The check valves are located after the mass-flow controllers to prevent the opposite flow through the MFC. The four mass-flow controllers are from Sevenstar (China) models CS-200, with nitrogen (both are 0–5 SLPM), helium (0–5 SLPM), and carbon dioxide (0–1 SLPM) with a linear response between 0 and 5 VDC, with an error lower than 0.5% in the flow scale.

(2) The VPSA column section consists of four shut-off valves, a regulating valve, a back-pressure regulator, two pressure transducers, a vacuum pump, two mass flow meters, two check valves, two thermocouples, and the concentric column made of stainless steel. The regulating valve, by which the vacuum blowdown flowrate can be regulated, is NUPRO. The back-pressure regulator is from TESCOM (MN, USA) (model 26-2300 series) working between 0 and 10300 kPa, with 2% accuracy and a maximum working temperature of 347.15 K. The vacuum pump is from ILMVAC (Germany), model MPC 301 Zp diaphragm type, allowing ultimate pressure of less than 8×10^{-5} kPa. The pressure transducers, shut-off valves and two check valves in this section have the same characteristics of those in the mixture section, except for the ranges of PT2 and PT3 are (−100–500 kPa) and (0–500 kPa), respectively. The concentric column has an inner-tube inner diameter of 25 mm and out-tube inner diameter of 55 mm. The inner tube is the adsorption column filled with adsorbents, and the annulus is filled circularly with water to keep the inner packed column at a specific temperature. The temperature of the water is controlled

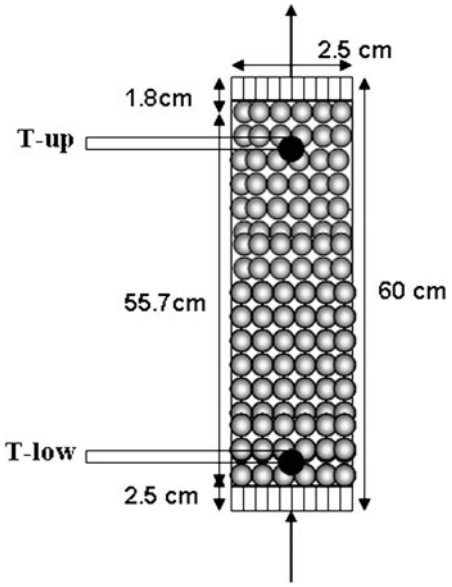

Fig. 2 Details of adsorption column used in the breakthrough and VPSA experiments

by thermostat baths, which is from CNSHP (China), model DC-2006. In this wok, 183.35 g AC beads were employed and the details of the column are shown in Fig. 2.

(3) The analytical section includes a gas chromatograph (GC) with an automatic valve sample system, a CO_2 infrared online analyzer, four shut-off valves and a computer with a data-acquisition system. This section is dedicated to analyzing on-line the composition of mixtures exiting the system. The acquisition software used is Forcecontrol 6.1, provided by KOSON (Shanghai, China). It can record the temperature, flow rate of all the mass-flow controllers, and the pressure from pressure transducers online. The gas chromatograph system is GC-950 (Shanghai, China) with thermal conductivity detector, and the column used in the GC was a CP-Poraplot Q with a flow rate of 7.0 mL/min of helium (used as carrier gas and as TCD reference gas) at room temperature. The infrared CO_2 analyzer is from JUNFANG, model GXH-1050E (Beijing, China).

All pipes are stainless steel of 3 mm diameter except for the vacuum pipeline is 6 mm, and all the connections are from Swagelok. All the gases used in the experiment were supplied by Shanghai Central Gases with purities of: $CO_2 >$ 99.999%, $N_2 >$ 99.999% and He > 99.999%.

2.2 Four-step vacuum pressure swing adsorption for CO_2 capture

The CO_2/N_2 separation by adsorption on AC beads is based on the equilibrium selectivity of CO_2 over N_2, $S_{CO_2/N_2} = 7.1$. To evaluate the performance of the pitched-based AC beads, a four-step Skarstrom-type cycle, including co-current pressurization with feed stream, feed, counter-current blowdown, and counter-current purge with N_2 was employed for CO_2 capture with the feed composition from 15–50% CO_2 balanced with N_2, which corresponds to the composition of flue gas. Before starting the experiments, the degassing of the adsorbent was carried out at 423 K for 12 h. Regeneration of the adsorbent for different experiments was performed under vacuum and purge with N_2 at desired temperature.

3 Theoretical

Due to bulk adsorption, non-isothermal behavior is expected considering the heat of adsorption/desorption and also the velocity of the gas inside the column will not be constant. To describe the dynamic behavior of the fixed bed filled with a bidisperse adsorbent, an axial dispersed plug flow mathematical model composed of material, momentum, and energy balances was employed. The complete mathematical model is shown in Table 1. Adsorption equilibrium of pure components of CO_2 and N_2 on AC beads were determined in a previous work and fitted with the Virial model (Shen et al. 2010). The crystal diffusivity of CO_2 and N_2 at low CO_2 concentration (determined in the linear region of the isotherms) were also reported before (Shen et al. 2010) as a function of temperature and described by:

$$\frac{D_c}{r_c^2} = \frac{D_{c,i}^0}{r_c^2} \exp\left(-\frac{E_{a,i}}{R_g T}\right) \tag{1}$$

where $D_{c,i}^0$ is the limiting diffusivity at infinite temperature and $E_{a,i}$ is the activation energy.

The adsorption equilibrium parameters of the Virial equation for CO_2 and N_2 are given in Table 2. Kinetics of adsorption was expressed by the bilinear driving force (bi-LDF) model for diffusion both in macropores and in micropores. Moreover, no mass, heat, or velocity gradients in the radial direction are considered. The axial dispersion groups $\varepsilon D_{ax}/D_{m,i}$, λ/k_g, and the Sherwood and Nusselt numbers, respectively, are calculated with the Wakao and Funazkri correlations (Wakao and Funazkri 1978), as suggested by Yang (1987). All properties in the bulk gas phase, i.e. viscosity, thermal gas conductivity, and molecular diffusion, are calculated with the reference conditions and then corrected locally by temperature and pressure according to Lu and Rodrigues (1994). The boundary conditions for the pressurization with feed, feed, counter-current blown and purge with N_2 are shown in Table 3. During the pressurization/depressurization steps, an exponential valve equation type is used following the experimental data (Lu and Rodrigues 1994).

This mathematical model has been used in the simulation of fixed-bed behavior and pressure swing adsorption applications of different mixtures showing very good agreement

Table 1 Mathematical model used to simulate fixed-bed experiments and the VPSA process for CO_2 capture with AC beads

Component mass balance	$\varepsilon_c \frac{\partial C_i}{\partial t} = \frac{\partial}{\partial z}\left(\varepsilon_c D_{ax,i} C_T \frac{\partial y_i}{\partial z}\right) - \frac{\partial (u C_i)}{\partial z} - (1-\varepsilon_c)\frac{a' k_{f,i}}{Bi_i+1} \times (C_i - \langle c_i \rangle)$ $i = 1, \ldots, n$
LDF equation for the macropore/micropore	$\varepsilon_p \frac{\partial \overline{c_i}}{\partial t} + \rho_p \frac{\partial \overline{\langle q_i \rangle}}{\partial t} = \varepsilon_p \frac{15 D_{p,i}}{R_p^2} \frac{Bi_i}{Bi_i+1}(C_i - \overline{c_i})$ $\frac{\partial \overline{\langle q_i \rangle}}{\partial t} = \frac{15 D_{c,i}}{r_c^2}(\langle q_i^* \rangle - \overline{\langle q_i \rangle})$
Gas phase energy balance	$\varepsilon_c C_T \tilde{C}_v \frac{\partial T_g}{\partial t} = \frac{\partial}{\partial z}\left(\lambda \frac{\partial T_g}{\partial z}\right) - u C_T \tilde{C}_p \frac{\partial T_g}{\partial z} + \varepsilon_c R_g T_g \frac{\partial C}{\partial t}$ $- (1-\varepsilon_c) a h_f (T_g - T_s) - \frac{2 h_w}{R_w}(T_g - T_w)$
Solid phase energy balance $= (1-\varepsilon_c)\varepsilon_p R_g T_S \frac{\partial \langle c_i \rangle}{\partial T} + \rho_b \sum_{i=1}^{n}(-\Delta H_i)\frac{\partial \overline{\langle q_i \rangle}}{\partial t} + (1-\varepsilon_c) a' h_f (T_g - T_s)$	$(1-\varepsilon_c)\left[\varepsilon_p \sum_{i=1}^{n} \langle c_i \rangle \tilde{C}_{vi} + \rho_p \sum_{i=1}^{n} \overline{\langle q_i \rangle} \tilde{C}_{v,ads,i} + \rho_p \tilde{C}_{ps}\right] \frac{\partial T_s}{\partial t}$
Wall energy balance	$\rho_w \tilde{C}_{pw} \frac{\partial T_w}{\partial t} = \alpha_w h_w (T_g - T_w) - \alpha_{w1} U (T_w - T_\infty)$
Ergun equation	$-\frac{\partial P}{\partial z} = \frac{150 \mu_g (1-\varepsilon_c)^2}{\varepsilon_c^3 d_p^2} u + \frac{1.75(1-\varepsilon_c)\rho_g}{\varepsilon_c^3 d_p} \lvert u \rvert u$
Virial extended isotherm	$P_i = \frac{q_i}{K_{Hi}} \exp\left(\frac{2}{S}\sum_{j=1}^{N} A_{ij} q_j + \frac{3}{2S^2}\sum_{j=1}^{N}\sum_{j=1}^{N} B_{ijk} q_j q_k\right)$
Biot number	$Bi_i = R_p k_{f,i} / 5 \varepsilon_p D_{p,i}$
Sherwood number	$\varepsilon D_{ax} / D_{m,i} = 20 + 0.5 Sc_i \mathrm{Re}$
Nusselt number	$\lambda / k_g = 7 + 0.5 \mathrm{Pr}\,\mathrm{Re}$

Table 2 Adsorption equilibrium and kinetic parameters of CO_2 and N_2 on AC beads

Gas	CO_2	N_2
K_∞ [mol/(kg·kPa)]	3.41×10^{-6}	2.38×10^{-6}
$(-\Delta H^0)$ [kJ/mol]	23.17	18.11
A_0 [kg/mol]	6.889	–2.017
A_1 [(kg·K)/mol]	–0.0871	688.392
B_0 [(kg/mol)$_2$]	0.0244	0.348
B_1 [(kg/mol)^2·K]	–8.652	–105.164
$D_{c,i}^0 / r_c^2$ [s^{-1}]	12.995	9.492
$E_{a,i}$ [kJ/mol]	18.050	12.391

between predictions and experimental data (Da Silva et al. 1999; Grande et al. 2008). The simulations were performed with gPROMS (PSE Enterprise, UK) using the orthogonal collocation on finite elements (OCFEM) with 50 finite elements and two interior collocation points in each element of the adsorption bed.

The performance of the VPSA experiments and simulations was evaluated according to three basic parameters: purity and recovery of product and unit productivity of the VPSA. They are defined by:

$$\text{Purity} = \frac{\int_0^{t_{blow}} C_{CO_2} u|_{Z=0}\, dt + \int_0^{t_{purge}} C_{CO_2} u|_{Z=0}\, dt}{\int_0^{t_{blow}} (C_{CO_2}+C_{N_2}) u|_{Z=0}\, dt + \int_0^{t_{purge}} (C_{CO_2}+C_{N_2}) u|_{Z=0}\, dt} \quad (2)$$

$$\text{Recovery} = \frac{\int_0^{t_{blow}} C_{CO_2} u|_{Z=0}\, dt + \int_0^{t_{purge}} C_{CO_2} u|_{Z=0}\, dt}{\int_0^{t_{feed}+t_{press}} C_{CO_2} u|_{Z=0}\, dt} \quad (3)$$

$$\text{Productivity} = \frac{CO_2 \textit{ obtained in blowdown} + CO_2 \textit{ obtained in purge step}}{t_{cycle} w_{ads}} \quad (4)$$

4 Results and discussion

4.1 Fixed-bed experiments

Before starting with VPSA experiments, breakthrough experiments were performed in order to determine the predictive capabilities of the mathematical model. These experiments are also valuable to determine some parameters such as the heat transfer coefficient at the wall (h_w) and external convective film transfer coefficient (U), which were fitted in the program for future use in VPSA simulations. Those parameters were firstly estimated by empirical correlations assuming that the fluid is stagnant and then fixed according to the experimental data. Breakthrough experiments with the feed flowrate of (1.0–3.0) SLPM and feed composition of (15–50)% CO_2 balanced with N_2 at (131.325–324.24) kPa and (303–333) K were carried out in order to verify the effect of feed flowrate, feed composition, operating pressure and temperature on the adsorption step and to check the parameters at different conditions. Moreover, breakthroughs at the same experimental conditions were performed to see the repeatability of the experiments. Details of the parameters were shown in Table 4. Since the radial diffusion and heat effect were not taken into account in the mathematical model, the lab-scale column was designed with small diameter to minimize these effects. It is also worth to notice that a large scale system is usually adiabatic, not cooled. However, the methodology reported here can also work in the adiabatic systems with the change of heat transfer parameters.

The experimental results showed that the mathematical model can describe well the breakthrough curves and temperature histories at various operating conditions. As an example, Fig. 4 shows the results of the experiments carried

Table 3 Boundary conditions for VPSA model

Step I: Pressurization with feed	
Inlet, $z = 0$	Outlet, $z = L$
$P(t)\|_{z+} = P(0)\|_{z+} + (P(t_I)\|_{z-} - P(0)\|_{z+})[1 - \exp(-M_1 t_I)]$	$u_i(L) = 0$
$-\frac{\varepsilon_c D_{ax,i}}{u_i(0)} \frac{\partial y(i,0)}{\partial z}\|_{z+} + y(i,0)\|_{z+} - y(i,0)\|_{-} = 0$	$\frac{\partial y(i,L)}{\partial z}\|_{z-} = 0$
$-\lambda \frac{\partial T_g(0)}{\partial z}\|_{z+} + u_i C_t \tilde{C}_p T_g(0)\|_{z+} - u_i C_t \tilde{C}_p T_g(0)\|_{z-} = 0$	$\frac{\partial T_g(L)}{\partial z}\|_{z-} = 0$
Step II: Feed	
Inlet, $z = 0$	Outlet, $z = L$
$u_i(0)C(i,0)\|_{z+} = u_i(0)C(i,0)\|_{z-}$	$P\|_{z-} = P\|_{z+}$
$-\frac{\varepsilon_c D_{ax,i}}{u_i(0)} \frac{\partial y(i,0)}{\partial z}\|_{z+} + y(i,0)\|_{z+} - y(i,0)\|_{z-} = 0$	$\frac{\partial y(i,L)}{\partial z}\|_{z-} = 0$
$-\lambda \frac{\partial T_g(0)}{\partial z}\|_{z+} + u_i C_t \tilde{C}_p T_g(0)\|_{z+} - u_i C_t \tilde{C}_p T_g(0)\|_{z-} = 0$	$\frac{\partial T_g(L)}{\partial z}\|_{z-} = 0$
Step III: Counter-current blowdown	
Outlet, $z = 0$	Inlet, $z = L$
$P(t)\|_{z+} = P(0)\|_{z+} + [P(t_{III})\|_{z-} - P(0)\|_{z+}][1 - \exp(-M_2 t_{III})]$	$u_i(L) = 0$
$\frac{\partial y(i,0)}{\partial z}\|_{z+} = 0$	$\frac{\partial y(i,L)}{\partial z}\|_{z-} = 0$
$\frac{\partial T_g()}{\partial z}\|_{z+} = 0$	$\frac{\partial T_g(L)}{\partial z}\|_{z-} = 0$
Step IV: Counter-current purge (N_2)	
Outlet, $z = 0$	Inlet, $z = L$
$P(0) = P_{\text{exit}}$	$u_i(L)C(i,L)\|_{z+} = u_i(L)C(i,L)\|_{z-}$
$\frac{\partial y(i,0)}{\partial z}\|_{z+} = 0$	$-\frac{\varepsilon_c D_{ax,i}}{u_i(L)} \frac{\partial y(i,L)}{\partial z}\|_{z-} + y(i,L)\|_{z-} - y(i,L)\|_{z+} = 0$
$\frac{\partial T_g(0)}{\partial z}\|_{z+} = 0$	$\lambda \frac{\partial T_g(L)}{\partial z}\|_{z-} + u_i C_t \tilde{C}_p T_g(L)\|_{z-} - u_i C_t \tilde{C}_p T_g(0)\|_{z+} = 0$

Table 4 Details of equipment and adsorbent properties used for CO_2/N_2 separation on AC beads

Column parameters		Adsorbent parameters	
Column length, m	0.557	Adsorbent specific area, m^2/kg	845.87
Inner column radius, m	0.025	Pellet diameter, m	$(1–1.18)\times10^{-3}$
Column porosity	0.32	Pellet density, kg/m^3	984.3
Bulk density, kg/m^3	670.6	Pellet porosity	0.506
Wall density, kg/m^3	8238	Pellet tortuosity	2.0
Specific heat of column wall, J/(kg·K)	500	Solid specific heat, J/(kg·K)	850

out exactly at the same conditions, from which we can observe that the breakthrough curves are practically the same indicating that reproducible results were obtained. It was also confirmed that the values of h_w and U were almost the same under different experimental conditions and they were 50 and 100, respectively.

4.2 Four-step VPSA experiments

After the fixed-bed runs, a group of VPSA experiments was carried out to evaluate the performance of this new adsorbent (AC beads). An open-ended design of the four-step cycle to be used for CO_2/N_2 separation in the laboratory unit described before (with column length and volume already specified) has the following operating and process parameters: T_{feed}, Q_{pres}, Q_{feed}, Q_{purge}, P_{feed}, P_{low}, t_{pres}, t_{feed}, t_{blow}, t_{purge} and feed composition. All these parameters may affect the performance of the VPSA cycles. The optimization of VPSA process is very difficult, particularly when they are related by a system of partial differential equations. In this work, the effect of most operating parameters was studied. Table 5 shows the main operating conditions and the performance of the experimental VPSA runs. As we can see from the breakthrough curves, the loading capacity of the column decreases significantly with the increase of operating temperature. In the VPSA runs, the operating temperature was fixed at 303 K, except for VPSA 8 and VPSA 9. The typical characteristics of a flue gas from a coal-fired power station are: 15% of CO_2, atmospheric pressure and possibility to cool down to near ambient temperature. Therefore, VPSA 1 was fixed at these conditions and other VPSA runs were per-

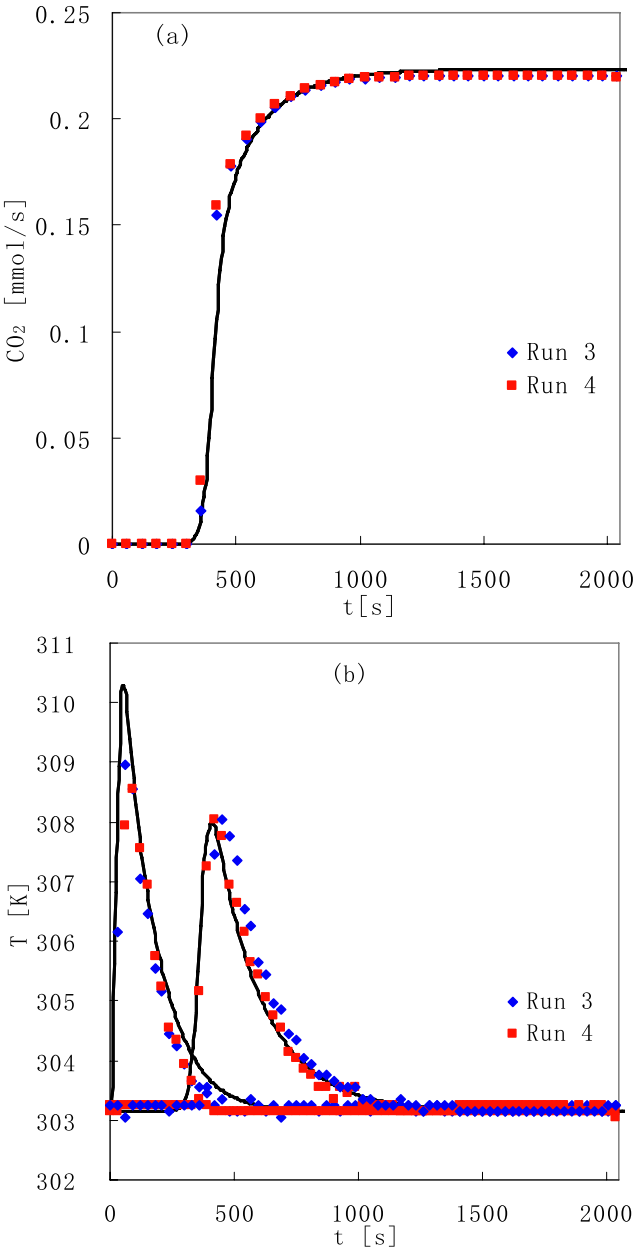

Fig. 3 Repeatability of breakthrough curves of CO_2/N_2 in AC beads: (**a**) CO_2 molar flowrate and (**b**) temperature histories at the same experimental conditions. *Solid lines* are theoretical model predictions, and *solid points* are experimental values

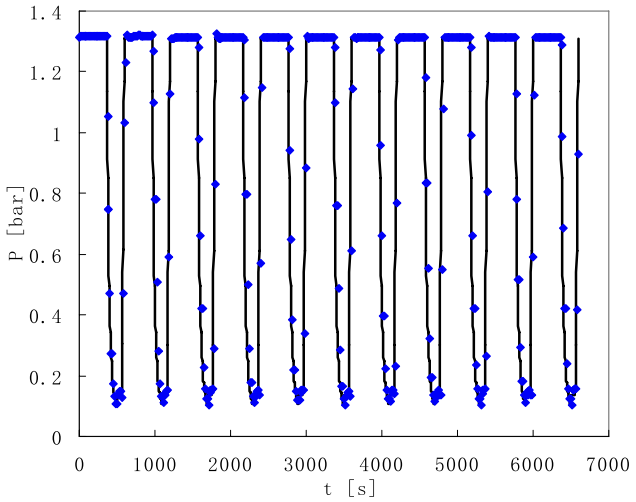

Fig. 4 Experimental and simulated pressure history at the exit end of the VPSA process (VPSA 1). *Solid lines* are theoretical model predictions, and *solid points* are experimental values

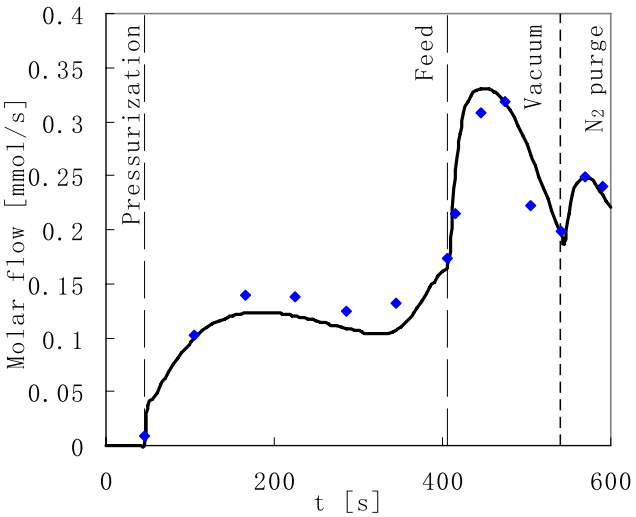

Fig. 5 Experimental and simulated molar flow rate of CO_2 at the exit end of the VPSA process in cyclic steady state operation, VPSA 1. *Solid lines* are theoretical model predictions, and *solid points* are experimental values

formed to compare the performance with it. According to the breakthrough curve of Run 3, the feed time was fixed at 360 s for VPSA 1. To be compared with VPSA 1, the feed time of the other VPSA runs was all fixed at 360 s.

4.2.1 Initial run of VPSA cycles

Before studying the effects of the different parameters, it is convenient to give an example of an experimental run obtained in a VPSA experiment using AC beads. For this purpose, VPSA 1 was used as example and to compare experimental and predicted results. Figures 4–6 show the main experimental results and simulated values for VPSA 1 (Table 5). In Fig. 4, we can see that the curve agrees quite well with the experimental data. In the first cycle, the initial pressure is P_{feed}, since the column was filled with nitrogen at the beginning of the experiments. Then follow the steps of feed, counter-current blowdown, N_2 purge and pressurization with feed. After the first cycle, the pressure history during each cycle is repeated, until the other operating variables achieve the cyclic steady-state condition.

Table 5 VPSA experiments for CO_2 capture from flue gas on AC beads

Case	T [K]	P_{feed} [kPa]	P_{low} [kPa]	t_{pres} [s]	t_{blow} [s]	Q_{feed} [SLPM]	y_{CO_2} [%]	Purity [%]	Recovery [%]	Productivity [mol/(kg·h)]
VPSA 1	303	131.325	10	45	135	2.0	0.15	48.56	55.35	1.64
VPSA 2	303	131.325	10	98	130	1.0	0.15	43.58	85.05	1.31
VPSA 3	303	131.325	10	30	135	3.0	0.15	50.35	40.70	1.76
VPSA 4	303	131.325	5	45	270	2.0	0.15	53.75	66.03	1.59
VPSA 5	303	131.325	3	46	330	2.0	0.15	54.06	69.05	1.54
VPSA 6	303	131.325	10	48	165	2.0	0.25	67.79	55.81	2.63
VPSA 7	303	131.325	10	60	285	2.0	0.50	90.06	57.80	4.64
VPSA 8	313	131.325	10	39	110	2.0	0.15	47.89	49.81	1.53
VPSA 9	333	131.325	10	32	90	2.0	0.15	48.18	41.76	1.32
VPSA 10	303	202.65	10	67	190	2.0	0.15	57.83	75.48	2.00
VPSA 11	303	324.24	10	126	240	2.0	0.15	63.04	96.16	2.42
VPSA 12	303	202.65	10	94	420	2.0	0.50	93.70	78.23	5.56

Note: For all the VPSA experiments, $t_{feed} = 360$ s, $t_{purge} = 60$ s, $Q_{purge} = 0.15$ SLPM

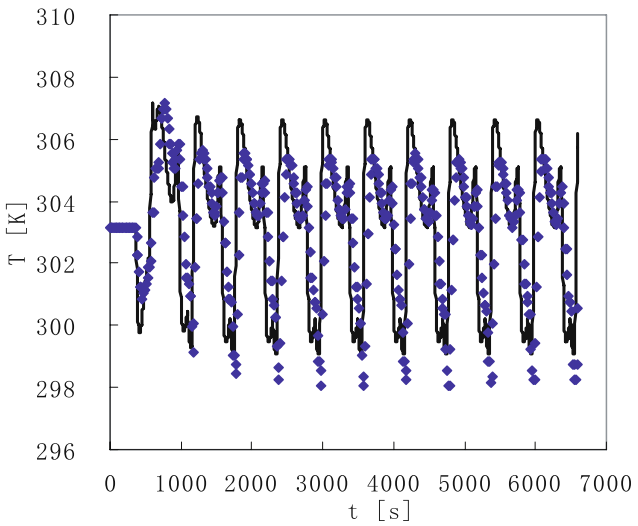

Fig. 6 Experimental and simulated temperature histories measured 0.507 m from column inlet, VPSA 1. *Solid lines* are theoretical model predictions, and *solid points* are experimental values

Figure 5 shows the molar flow rate for cycles 6–11 where no significant variation of molar flow rate was experimentally detected and thus we may assume that represent the behavior of the cyclic steady state. The experimental and simulation results agree quite well. Minor differences between the experimental and simulated molar flow rates, may be due to the fact that the experimental values obtained from the experimental unit are affected by the dynamics of the back pressure, the vacuum pump that works during the countercurrent blowdown step, while in the simulation the values computed are without the interference of other equipment. In Fig. 6, it can be observed that the temperature history stabilizes around a cyclic steady-state behavior after 6 cycles. Since massive breakthrough of CO_2 in run VPSA 1 and in many others, the recovery was quite small.

4.2.2 *Effect of operating parameters on VPSA performance*

In this subsection, the effects of total feed flowrate, feed composition, feed pressure, operating temperature and vacuum pressure were experimentally studied. The operating conditions are listed in Table 5.

The experimental results are shown in Fig. 7. As shown in Fig. 7(a), CO_2 purity increased from 43.58% to 50.35% when the feed flowrate increased from 1.0 SLPM to 3.0 SLPM. Since the adsorption time is the same, increasing feed flowrate caused the increase of adsorption zone resulting in the increasing of CO_2 purity. However, the CO_2 recovery decreased from 85.05% to 40.70% due to the increase of feed flowrate, which is mainly due to the larger CO_2 lost when the feed flowrate is higher.

The CO_2 concentration in different streams where CO_2 capture can be employed ranges from 15% to 25% (IPCC report 2005) for different sources. In order to study the effect of feed concentration on the performance of VPSA experiments, the feed gas concentration was varied from 15% to 50% while keeping the other parameters the same with VPSA 1. The main results are shown in Fig. 7(b). We can see that both the purity and recovery of the process increase with feed concentration, as expected.

In the VPSA process, the power consumption of the blower is one of the main components of total cost. High adsorption pressure results in high power consumption of the blower, thus, the effect of the feed pressure was studied, as shown in Fig. 7(c). While the feed pressure rises from 131.325 kPa to 324.24 kPa, the purity of CO_2 increase, too,

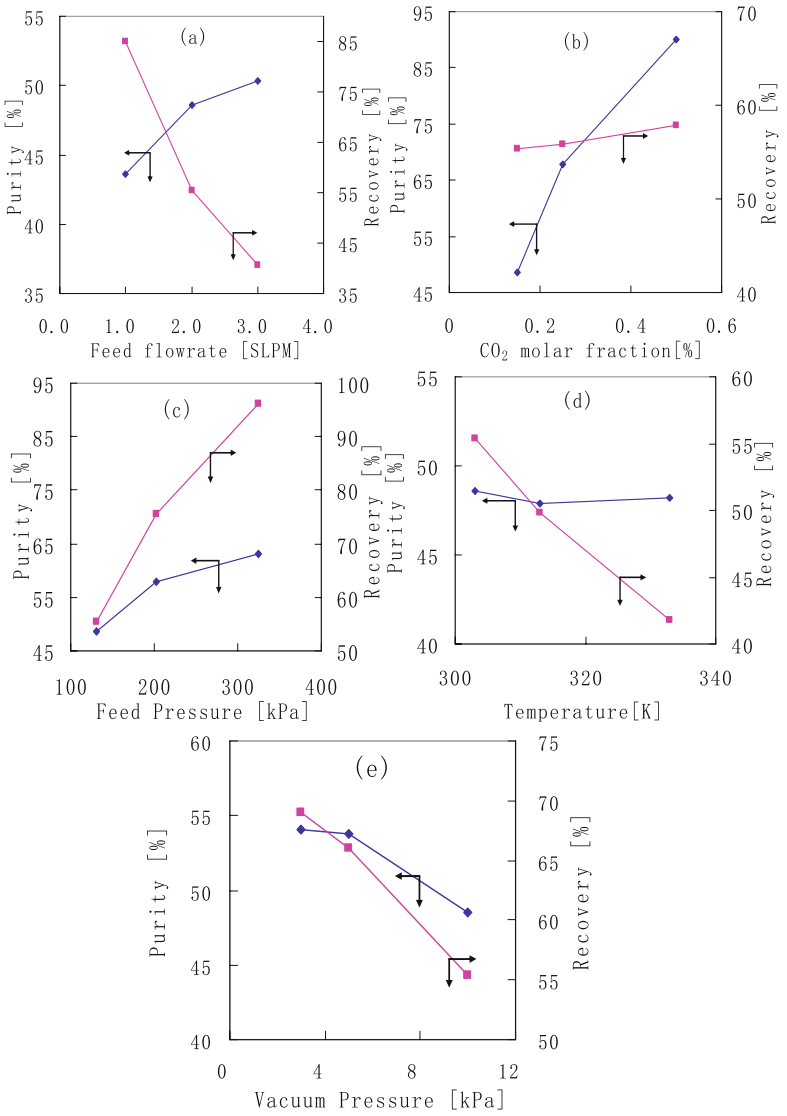

Fig. 7 Effect of the operating parameters on the VPSA performance, using AC beads as adsorbent. (**a**) Total feed flowrate; (**b**) CO_2 concentration in feed; (**c**) feed pressure; (**d**) operating temperature; (**e**) vacuum pressure

as a direct result of more CO_2 being adsorbed and then released in the product. Although co-current depressurization was introduced in runs of VPSA 10 and 11 after the feed step, which may cause some loss of CO_2, its recovery still increase with the rise of feed pressure. It means that the main step of CO_2 loss is not in the co-current depressurization but the feed step. For the typical composition of flue gas (15% CO_2), even when the feed pressure is up to 324.24 kPa, the purity is still low (63.04%) using the Skarstrom-type four-step VPSA process.

A flue gas stream may be available over a range of temperatures depending on the design and process operation of the power generation system. There exists the case in the coal-fired power plant, where the temperature of the flue gas is at the range of 303–333 K after the heat exchanger and wet desulphurization of the flue gas. In runs of VPSA 3, 8 and 9, the impact of operating temperature on the process performance was investigated. Figure 7(d) indicates that as the temperature increases from 303 K to 333 K, both the recovery and productivity decreases while the purity has no significant difference. The reduction in productivity and recovery is caused by the reduction in the loading capacity of the column when the temperature increases, and therefore by the reduction in the amount of CO_2 extracted from column during the counter-current blowdown step.

The selection of evacuation pressure is an important variable since it governs the energy performance of the system. However, when a flue gas with atmospheric pressure (containing 10–15 kPa CO_2) is employed for adsorption, low evacuation pressure will be necessary to desorb CO_2. In Fig. 7(e), it can be observed that both the purity and recovery reduces with the increase of vacuum pressure. A small increase of vacuum pressure from 5 kPa to 10 kPa reduces the performance of the process significantly.

As discussed above, with a four-step Skarstrom VPSA process using AC beads it was not possible to reach CO_2

purity higher than 95%. To improve the VPSA performance, there are some ways such as decreasing the vacuum pressure, increasing the feed pressure and increasing the feed composition. However, these alternatives will result in increased energy consumption. Instead of changing operating variables and increase the energy consumption of the system, it would be desirable to modify the cycle and include steps such as rinse with concentrated CO_2 and even pressure equalization to save some energy. Another possibility is assumed that a two-stage VPSA process is used to capture CO_2 from flue gas, that is, the flue gas was firstly separated by the four-step Skarstrom-type VPSA process, taking VPSA 1 as an example (a purity of 48.56% and recovery of 88.35% is obtained), and then the product (Y_{CO_2} is almost 50%) is compressed to 2 atm and separated again by the four-step VPSA process (Park et al. 2002). For this reason, experiment of VPSA 12 was performed. As shown in Table 5, a purity of 93.7% with recovery of 78.23% can be obtained in the second separation which is quite close to target of 95% purity. By this way, the power consumption for compressing the product is much less than compressing the flue gas directly. On the other hand, the feed composition increases for the second stage VPSA separation.

Considering the un-treated flue gas, there have been some studies examining the effect of water, SOx, NOx on the adsorption of CO_2 (Reddy et al. 2008; Zhang et al. 2009; Li et al. 2009). Water is usually adsorbed prior to other adsorbates due to its strong polarity. As reported, zeolite materials have a large adsorption capacity for water and it competes for sites where CO_2 adsorbs, which makes CO_2 capacity decrease significantly. SOx is reported to have reactions with basic sites on adsorbent materials. NO can be oxidized to $NO_2/N_2O_3/N_2O_5$ and eventually react with the adsorbent (Rouf and Eic 1998; Mello and Eic 2002). The pressure-swing reversible adsorption capacity for these impurities is very small (Sultana et al. 2004; Reddy et al. 2008). Adsorption column with multi-layer adsorbents was introduced to resolve the problem by removing the impurities one by one. However, the interactions of $CO_2/H_2O/SOx/NOx$ in typical flue gas with adsorbents are very complex. Our future work will examine these interactions and their effect on the VPSA process performance systematically.

5 Conclusions

Experimental fixed-bed and vacuum pressure swing adsorption (VPSA) experiments were shown for the capture of CO_2 from flue gas using AC beads, which was synthesized by our cooperators in our laboratory. Breakthrough experiments were carried out at different conditions in order to verify the effect of feed flowrate, feed pressure, feed composition and operating temperature on the adsorption step and to fit the parameters for simulation model. Based on the breakthrough experiments, a skarstrom-type VPSA with four-step (pressurization with feed, feed, counter-current blowdown, pure with N_2) was employed to evaluate the new adsorbent. Various parameters such as feed total flowrate, feed composition, feed pressure, operating temperature and vacuum pressure were studied experimentally. According to the experimental research, the mathematical model proposed in this work could predict the VPSA behavior at the condition of isothermal operation without the effects of water and other impurities.

Using the AC beads, feeding with 15% CO_2 at 303 K and 131.325 kPa, purity of 48.56% with recovery of 55.35% was obtained by using the four-step VPSA process in a single column. Increasing feed pressure to 202.65 kPa, a CO_2 purity of 93.70% with 78.23% of recovery was obtained. As other commercial activated carbons, it may also be expensive to use this new AC beads to capture CO_2 from flue gas by VPSA process.

Acknowledgements The authors are grateful for the financial support of China 863 program (Grant No. 2008AA062302), Shanghai international cooperation project (Grant No. 08160704000), Shanghai Pujiang Talent program (Grant No. 08PJ14034) and the fellowship from China Scholarship Council (CSC) for the stay of C.S. at LSRE. The authors also acknowledge Professor Ling Licheng to provide the activated carbon beads.

References

Aaron, D., Tsouris, C.: Separation of CO_2 from flue gas: a review. Sep. Sci. Technol. **40**, 321–348 (2005)

Chaffee, A.L., Knowles, G.P., Liang, Z., Zhany, J., Xiao, P., Webley, P.A.: CO_2 capture by adsorption: materials and process development. Int. J. Greenhouse Gas Control **1**, 11–18 (2007)

Chue, K.T., Kim, J.N., Yoo, Y.J., Cho, S.H., Yang, R.T.: Comparison of activated carbon and zeolite 13X for CO_2 recovery from flue-gas by pressure swing adsorption. Ind. Eng. Chem. Res. **34**, 591–598 (1995)

Ciferno, J.P., Fout, T.E., Jones, A.P., Murphy, J.T.: Capturing carbon from existing coal-fired power plants. Chem. Eng. Prog. **105**, 33–41 (2009)

Da Silva, F.A., Silva, J.A., Rodrigues, A.E.: A general package for the simulation of cyclic adsorption processes. Adsorption **5**(3), 229–244 (1999)

Diagne, D., Goto, M., Hirose, T.: Parametric studies on CO_2 separation and recovery by a dual reflux PSA process consisting of both rectifying and stripping sections. Ind. Eng. Chem. Res. **34**, 3083–3089 (1995)

Grande, C.A., Lopes, F.V.S., Ribeiro, A.M., Loureiro, J.M., Rodrigues, A.E.: Adsorption of off-gases from steam methane reforming (H_2, CO_2, CH_4, CO and N_2) on activated carbon. Sep. Sci. Technol. **43**, 1338–1364 (2008)

Ho, M.T., Allinson, G.W., Wiley, D.E.: Reducing the cost of CO_2 capture from flue gases using pressure swing adsorption. Ind. Eng. Chem. Res. **47**, 4883–4890 (2008)

Kikkinides, E.S., Yang, R.T., Cho, S.H.: Concentration and recovery of CO_2 from flue-gas by pressure swing adsorption. Ind. Eng. Chem. Res. **32**, 2714–2720 (1993)

Li, G., Xiao, P., Webley, P.A., Zhang, J., Singh, R.: Competition of CO_2/H_2O in adsorption based CO_2 capture. Energy Procedia **1**, 1123–1130 (2009)

Liu, Z.C., Ling, L.C., Qiao, W.M., Liu, L.: Preparation of pitch-based spherical activated carbon with developed mesopore by the aid of ferrocene. Carbon **37**, 663–667 (1999)

Lu, Z.P., Rodrigues, A.E.: Pressure swing adsorption reactors: simulation of three-step one-bed process. AIChE J. **40**, 1118–1137 (1994)

Mello, M., Eic, M.: Adsorption of sulphur dioxide from pseudo binary mixtures on hydrophobic zeolites: modeling of breakthrough curves. Adsorption **4**, 279–289 (2002)

Park, J.-H., Beum, H.-T., Kim, J.-N., Cho, S.-H.: Numerical analysis on the power consumption of the PSA process for recovering CO_2 from flue gas. Ind. Eng. Chem. Res. **41**, 4122–4131 (2002)

Radosz, M., Hu, X.D., Krutkramelis, K., Shen, Y.Q.: Flue-gas carbon capture on carbonaceous sorbents: toward a low-cost multifunctional carbon filter for "Green" energy producers. Ind. Eng. Chem. Res. **47**, 3783–3794 (2008)

Reddy, M.K.R., Xu, Z.P., Lu, G.Q. (Max), Diniz da Costa, J.C.: Effect of SO_x adsorption on layered double hydroxides for CO_2 capture. Ind. Eng. Chem. Res. **47**, 7357–7360 (2008)

Rouf, S.A., Eic, M.: Adsorption of SO_2 from wet mixtures on hydrophobic zeolites. Adsorption **4**, 25–33 (1998)

Shen, C., Grande, C.A., Rodrigues, A.E.: Adsorption equilibria and kinetics of CO_2 and N_2 on activated carbon beads. Chem. Eng. J. **160**, 398–407 (2010)

Sultana, A., Habermacher, D.D., Kirschhock, C.E.A., Martens, J.A.: Adsortive separation of NO_x in presence of SO_x from gas mixtures simulating lean burn engine exhaust by pressure swing process on Na-Y zeolite. Appl. Catal. B: Environ. **48**, 65–76 (2004)

Wakao, N., Funazkri, T.: Effect of fluid dispersion coefficients on particle-to-fluid mass transfer coefficients in packed beds. Chem. Eng. Sci. **33**, 1375 (1978)

Working Group III of the Intergovernmental Panel on Climate Change: IPCC Special Report on Carbon Dioxide Capture and Storage. Cambridge University Press, Cambridge (2005)

Yang, R.T.: Gas Separation by Adsorption Processes. Butterworths, Boston (1987)

Zhang, J., Xiao, P., Li, G., Webley, P.A.: Effect of flue gas impurities on CO_2 capture performance from flue gas at coal-fired power stations by vacuum swing adsorption. Energy Procedia **1**, 1115–1122 (2009)

Zhang, J., Webley, P.A., Xiao, P.: Effect of process parameters on power requirements of vacuum swing adsorption technology for CO_2 capture from flue gas. Energy Convers. Manag. **49**, 346–356 (2008)